

## ARTICLE OPEN

Incommensurate charge-stripe correlations in the kagome superconductor  $\text{CsV}_3\text{Sb}_{5-x}\text{Sn}_x$ Linus Kautzsch<sup>1</sup>, Yuzki M. Oey<sup>1</sup>, Hong Li<sup>2</sup>, Zheng Ren<sup>2</sup>, Brenden R. Ortiz<sup>1</sup>, Ganesh Pokharel<sup>1</sup>, Ram Seshadri<sup>1</sup>, Jacob Ruff<sup>3</sup>, Terawit Kongruengkit<sup>1</sup>, John W. Harter<sup>1</sup>, Ziqiang Wang<sup>2</sup>, Ilija Zeljkovic<sup>1</sup> and Stephen D. Wilson<sup>1</sup>✉

The class of  $\text{AV}_3\text{Sb}_5$  ( $A=\text{K, Rb, Cs}$ ) kagome metals hosts unconventional charge density wave states seemingly intertwined with their low temperature superconducting phases. The nature of the coupling between these two states and the potential presence of nearby, competing charge instabilities however remain open questions. This phenomenology is strikingly highlighted by the formation of two ‘domes’ in the superconducting transition temperature upon hole-doping  $\text{CsV}_3\text{Sb}_5$ . Here we track the evolution of charge correlations upon the suppression of long-range charge density wave order in the first dome and into the second of the hole-doped kagome superconductor  $\text{CsV}_3\text{Sb}_{5-x}\text{Sn}_x$ . Initially, hole-doping drives interlayer charge correlations to become short-ranged with their periodicity diminished along the interlayer direction. Beyond the peak of the first superconducting dome, the parent charge density wave state vanishes and incommensurate, quasi-1D charge correlations are stabilized in its place. These competing, unidirectional charge correlations demonstrate an inherent electronic rotational symmetry breaking in  $\text{CsV}_3\text{Sb}_5$ , and reveal a complex landscape of charge correlations within its electronic phase diagram. Our data suggest an inherent  $2\mathbf{k}_F$  charge instability and competing charge orders in the  $\text{AV}_3\text{Sb}_5$  class of kagome superconductors.

*npj Quantum Materials* (2023)8:37; <https://doi.org/10.1038/s41535-023-00570-x>

## INTRODUCTION

Charge correlations and the nature of charge density wave (CDW) order within the class of  $\text{AV}_3\text{Sb}_5$  ( $A=\text{K, Rb, Cs}$ ) kagome superconductors<sup>1–4</sup> are hypothesized to play a crucial role in the anomalous properties of these compounds. Hints of pair density wave superconductivity<sup>5,6</sup>, magnetochirality and nonreciprocal transport<sup>7,8</sup>, as well as orbital magnetism<sup>9–12</sup> in these compounds are all born out of a central CDW state<sup>13–15</sup>. The CDW order parameter itself is theorized to host both primary, real and secondary, imaginary components<sup>16</sup>, each of which is thought to play a role in the anomalous properties observed in  $\text{AV}_3\text{Sb}_5$  compounds.

The real component of the CDW state manifests primarily as a  $2 \times 2$  reconstruction within the kagome plane driven via a  $3\mathbf{q}$  distortion into either star-of-David (SoD) or (its inverse) trihexagonal (TrH) patterns of order<sup>17</sup>. In-plane distortions are further correlated between kagome layers<sup>13,18–20</sup>, either through correlated phase shifts of the same distortion type between neighboring layers, via alternation between distortion mode types, or a combination of both<sup>21</sup>.

The parent CDW state of  $\text{CsV}_3\text{Sb}_5$  forms a lattice whose average structure is comprised of a modulation between SoD and TrH distortion modes along the interlayer  $c$ -axis below  $T_{\text{CDW}}=94\text{ K}$ <sup>19,22,23</sup>. Locally, the CDW supercell arises from a nearly degenerate mixture of states with  $2 \times 2 \times 4$  and  $2 \times 2 \times 2$  cells whose selection is dependent upon subtle effects such as thermal history and strain conditions imparted during growth<sup>24,25</sup>. While the interlayer stacking details are a low energy feature susceptible to small perturbations, the dominant feature of the CDW in all cases is the  $2 \times 2$  reconstruction in the  $ab$ -plane, representing a commensurate charge modulation on the kagome lattice.

Upon cooling deeper into the CDW state, hints appear of a staged behavior within the in-plane charge modulation,

suggestive of another coexisting or competing CDW instability. Scanning tunneling microscopy (STM) measurements resolve commensurate, quasi-1D charge stripes that form near  $T \approx 60\text{ K}$  and coexist with the  $2 \times 2$  in-plane CDW order<sup>14</sup>, while transient reflectivity<sup>26</sup> and Raman measurements<sup>27</sup> also resolve a shift/new modes in the lattice dynamics near this same energy scale. Sb NQR and V NMR measurements further observe a chemical shift in this temperature regime<sup>28</sup>, demonstrating a structural response to a modified CDW order parameter—one potentially driven by competing CDW correlations.

Further supporting the notion of a nearby charge state competing with the parent CDW order is the rapid suppression of thermodynamic/transport signatures of the CDW state in  $\text{CsV}_3\text{Sb}_5$  under moderate pressure<sup>29,30</sup> or via small levels of hole-substitution<sup>31</sup>. By substituting  $\approx 6\%$  holes per formula unit, the CDW state seemingly vanishes in thermodynamic measurements, whereas superconductivity undergoes a nonmonotonic response and generates two superconducting domes. Understanding the evolution of charge correlations between these two domes stands to provide important insights into the origin of the unconventional coupling between CDW order and superconductivity reported in  $\text{CsV}_3\text{Sb}_5$ .

Here we track the evolution of charge correlations in  $\text{CsV}_3\text{Sb}_{5-x}\text{Sn}_x$  as holes are introduced via Sn-substitution and the in-plane  $2 \times 2$  CDW state is suppressed. X-ray diffraction data resolve that very light Sn-substitution ( $x=0.025$ ) suppresses CDW correlations, and the CDW immediately becomes short-ranged along the interlayer axis. Increased hole-doping reveals continued shortening of interlayer correlations and the suppression of in-plane  $2 \times 2$  CDW order; however, this suppression of commensurate  $2 \times 2$  order is accompanied by the emergence of competing quasi-1D, incommensurate charge correlations ( $x=0.15$ ). Parallel STM measurements also observe the persistence of low-

<sup>1</sup>Materials Department, University of California Santa Barbara, Santa Barbara, CA 93106, USA. <sup>2</sup>Department of Physics, Boston College, Chestnut Hill, MA 02467, USA. <sup>3</sup>CHESS, Cornell University, Ithaca, NY 14853, USA. ✉email: [stephendwilson@ucsb.edu](mailto:stephendwilson@ucsb.edu)

temperature quasi-1D charge stripes in the absence of  $2 \times 2$  CDW order<sup>32</sup>. Our data unveil a complex landscape of competing charge correlations that evolve across the superconducting domes of this material.

## RESULTS

### X-ray diffraction data and analysis

To understand the evolution of charge correlations across the electronic phase diagram of  $\text{CsV}_3\text{Sb}_{5-x}\text{Sn}_x$ , two Sn concentrations were chosen as shown in Fig. 1(a). The first  $x = 0.025$  concentration possesses both a superconducting state with an enhanced  $T_c$  and a clearly observable CDW transition as shown in Fig. 1(b), (c). The second  $x = 0.15$  concentration retains a SC phase transition but the thermodynamic signature of  $2 \times 2$  CDW order in susceptibility has vanished as shown in Fig. 1(d), (e).

Looking first at the  $x = 0.025$  crystal, maps of x-ray diffraction data were collected with representative data plotted in Fig. 2(a) and (b). Figure 2(a) plots scattering within the  $(H, K, 1.5)$ -plane. Reflections centered at  $(H, K) = (0.5, 0.5)$ -type positions indicate that the parent  $2 \times 2$  in-plane CDW order remains in the  $x = 0.025$  compound. However, interlayer correlations are altered. Fig. 2(c) plots scattering within the  $(H, 1.5, L)$ -plane, showing that  $c$ -axis

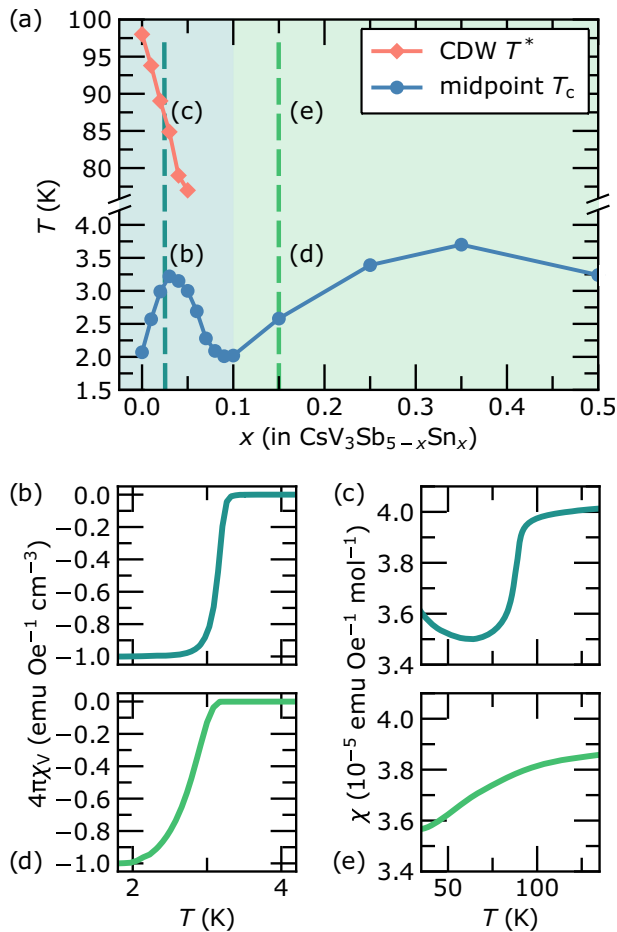


**Fig. 1 Evolution of electronic order in  $\text{CsV}_3\text{Sb}_{5-x}\text{Sn}_x$ .** **a** Electronic phase diagram of Sn-doped  $\text{CsV}_3\text{Sb}_5$  showing the evolution of both CDW and SC order with hole-doping in powder samples. Data are reproduced from ref. <sup>31</sup>. **b** and **c** Show susceptibility data characterizing the superconducting and CDW states of a crystal with the  $x = 0.025$  composition in the first SC 'dome' and **(d)** and **(e)** show susceptibility data characterizing the superconducting and CDW states of a crystal with the  $x = 0.15$  composition in the second SC 'dome'.

correlations shift to become substantially shorter-range and center primarily at the  $L = 0.5$  positions. This marks a suppression of  $2 \times 2 \times 4$  correlations in the undoped material and a transition into a short-range CDW state whose  $\mathbf{q}$  vectors match those of undoped  $(\text{K,Rb})\text{V}_3\text{Sb}_5$ <sup>13</sup>.

The in-plane correlation lengths associated with CDW peaks in the  $x = 0.025$  sample are slightly reduced, shortening from resolution-limited in the undoped material to  $\xi_H = 367 \pm 6$  Å. Interplane correlation lengths shorten dramatically, reducing to  $\xi_L = 70 \pm 2$  Å. CDW peak intensities and positions are symmetric with respect to  $\pm L$ , and Fig. 2(c) provides a narrower field of view for clarity. Weak reflections also appear at integer  $L$  positions with shorter correlation lengths  $\xi_L = 40 \pm 2$  Å. Similar weak, integer  $L$  reflections also appear in the undoped  $x = 0$  compound, and their presence likely reflects that interlayer correlations are heavily impacted by local minima upon rapid cooling<sup>24,25,27</sup>. The difference in correlation lengths between half-integer and integer  $L$  CDW reflections in the  $x = 0.025$  sample reflects two distinct patterns of  $c$ -axis modulation present prior to reaching a doping level where the CDW becomes truly two-dimensional.

At this small doping level, the immediate disappearance of  $L = 0.25$  type peaks demonstrates a reduction in the mixed character of CDW order and suggests a switch from a state with modulating SoD and TrH order into one with phase-shifted planes of a single distortion type, similar to  $(\text{K,Rb})\text{V}_3\text{Sb}_5$ <sup>22</sup>. This crossover into another CDW phase at light doping may drive the formation of the first SC dome in the phase diagram of  $\text{CsV}_3\text{Sb}_{5-x}\text{Sn}_x$ ; however a quantitative refinement of the isolated  $2 \times 2 \times 2$  CDW state will be required to further understand the mechanism.

Examining charge correlations outside of the nominal  $2 \times 2$  CDW phase boundary, x-ray scattering data for the  $x = 0.15$  sample are plotted in Fig. 3. Panels (a) and (b) show a representative schematic of the scattering and data in the  $(H, K, -0.5)$ -plane. Data collected at half-integer  $L$  values indicate a superposition of three quasi-1D patterns of charge scattering. This can be understood in a model of charge correlations forming preferentially along one unique in-plane axis (i.e.,  $H$  or  $K$ ), reducing the sixfold rotational symmetry to twofold, and forming three domains rotated by  $120^\circ$  in real space. These quasi-1D domains vanish upon warming as shown in Fig. 3(d), similar to CDW domain formation in the undoped  $x = 0$  system observed in optical and STM measurements<sup>9,14</sup>.

Looking at scattering from a single domain, charge correlations form an incommensurate state with  $\mathbf{q}_{\text{inc}} = 0.37$  along a preferred in-plane axis. This is illustrated by a representative cut along  $H$  plotted in Fig. 3(c). Within the  $(H, K)$ -plane, correlations along  $\mathbf{q}_{\text{inc}}$  are short-ranged with  $\xi_H = 66 \pm 2$  Å and are substantially longer-ranged orthogonal to the direction of modulation with  $\xi_K = 176 \pm 7$  Å (Fig. 2(e)). As shown in Fig. 3(f), the peak of these quasi-1D correlations is centered at the  $L = -0.5$  position with a short-correlation length of  $\xi_L = 18 \pm 1$  Å, reflecting an anti-phase modulation between neighboring kagome layers correlated only between neighboring V-planes. We note here that all of these charge density correlation lengths are substantially longer than the projected distance between Sn-dopants assuming an isotropic distribution. Analysis of scattering attributed to the other two domains is presented in Supplementary Figs. 1–4.

### Scanning tunneling microscopy data and analysis

To further investigate the local evolution of charge correlations, STM measurements were performed on the  $x = 0.15$  sample at  $T = 4.5$  K. Figure 4(a), (b) show STM topographs of the Sb surface over different fields of view where dark hexagonal defects correspond to individual Sn dopants. Counting these defects is consistent with the expected Sn concentration  $x = 0.15$ . Specifically, STM analysis counts Sn-dopants on the surface at a concentration between  $x = 0.08$  and  $x = 0.10$ , within the  $\approx 1$  atm

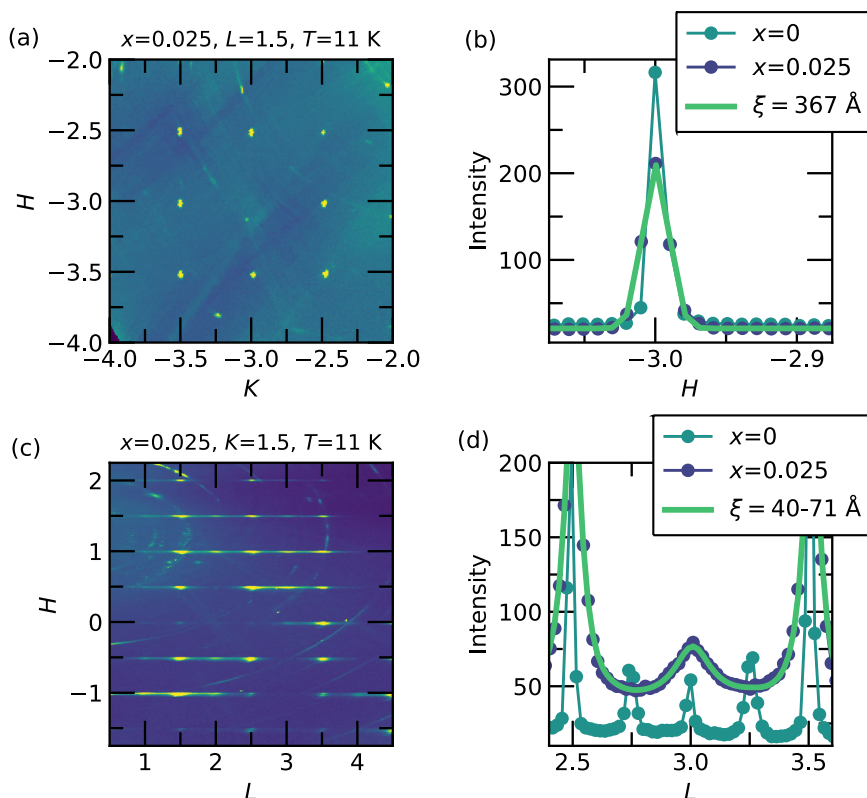


**Fig. 2** X-ray scattering from a  $x = 0.025$  crystal. **a** Map of x-ray scattering intensities in the  $(H, K, 1.5)$ -plane for the  $x = 0.025$  sample at  $T = 11$  K. **b** One dimensional  $H$ -cuts through the  $(-3, -2.5, 1.5)$  position for both  $x = 0$  and  $x = 0.025$ . Solid lines are Gaussian fits to the data. **c** Map of x-ray scattering intensities in the  $(H, 1.5, L)$  plane for the  $x = 0.025$  sample. **d** One-dimensional  $L$ -cuts along  $H = 1$  for both the  $x = 0$  and  $x = 0.025$  samples. Solid lines are pseudo-Voigt fits for the  $x = 0.025$  sample with the Gaussian component fixed to the instrument's resolution.

% resolution of EDS measurements. One-dimensional, stripe-like features are apparent in the STM topograph (Fig. 4(a) and (b)), which can be more easily quantified via the Fourier transform plotted in Fig. 4(c). In this Fourier map, quasi-1D correlations are observed along one of the atomic Bragg peak directions with a map-averaged  $\mathbf{q}_{\text{inc}} \approx 0.2$ , reminiscent of the previously identified  $4a_0$  charge stripes in the undoped system<sup>14</sup>. The superlattice peaks at the  $2 \times 2$  (or  $\mathbf{q}_{2\text{D-CDW}}$ ) CDW positions are notably absent. This is further demonstrated via the line cuts through the Fourier map along the three lattice directions, where no scattering peaks can be observed at  $2 \times 2$  positions (Fig. 4(d)).

To gain insight into the electronic band structure, quasiparticle interference (QPI) imaging is plotted in Fig. 4. Fourier transforms of STM  $dI/dV$  maps in Fig. 4(e)–(g) show the electron scattering and interference pattern as a function of increasing STM bias (binding energy). The dominant dispersive scattering wave vector is the nearly isotropic central circle (labeled  $\mathbf{q}_1$ ), which arises from scattering within the Sb  $p_z$  band that crosses through  $E_F$ . Hole-doping is predicted to be orbitally-selective and should preferentially dope this band<sup>31,33</sup>, pushing the bottom of the band closer to  $E_F$ . Figure 4 (h) shows the resulting dispersion of  $\mathbf{q}_1$ , where it can be seen that the bottom of the Sb  $p_z$  band has been pushed up from below  $-600$  meV in the  $x = 0$  parent system<sup>14</sup> to  $\approx -500$  meV in the  $x = 0.15$  sample. This is consistent with DFT expectations of hole-doping achieved via the replacement of in-plane Sb atoms with Sn.

The persistence of stripe-like correlations on the surface of the  $x = 0.15$  sample in the absence of the  $2 \times 2$  CDW state suggests that the interactions driving this surface order are linked to the formation of the quasi-1D order resolved in the bulk via x-ray scattering measurements. In STM data, the only charge correlations that break translational symmetry are inhomogeneous,

incommensurate stripes, and, diffraction measurements show that incommensurate charge modulations *should be present*. We therefore hypothesize that the quasi-1D correlations sampled in diffraction and STM data arise from the same instability, with the precise wave vector of the quasi-1D stripes modified by the surface in STM studies. The wave vector could be modified by potential surface doping due to the polar surface and removal of Cs for STM measurements or the correlations could be modified by surface strain. Future measurements will be required to prove the hypothesis that both quasi-1D correlations sampled in x-ray and STM measurements arise from a common origin.

Quasi-1D correlations were observed in STM measurements to pin at the surface below  $\approx 60$  K in undoped  $\text{CsV}_3\text{Sb}_5$ <sup>14</sup> and coherent, quasi-1D band features appear in the differential conductance  $dI/dV$  maps at low temperature<sup>34</sup>, reflective of a strong coupling between these correlations and the electronic structure. Estimates of the onset temperature of quasi-1D correlations in the  $x = 0.15$  sample show that they persist to 60 K and optical data suggest they form in a similar temperature range (Supplementary Fig. 5). We note here that the short-range nature of the charge-correlations in the  $x = 0.15$  sample means that there is no clear thermodynamic anomaly in heat capacity or magnetization data that makes their onset temperature readily apparent.

## DISCUSSION

The incommensurate character of the CDW correlations in the  $x = 0.15$  sample stresses the importance of electron-electron interactions in this regime of the phase diagram. A  $2\mathbf{k}_F$  nesting instability can, in principle, arise once the  $2 \times 2$  reconstruction of the original Fermi surface is lifted and the Fermi level is shifted

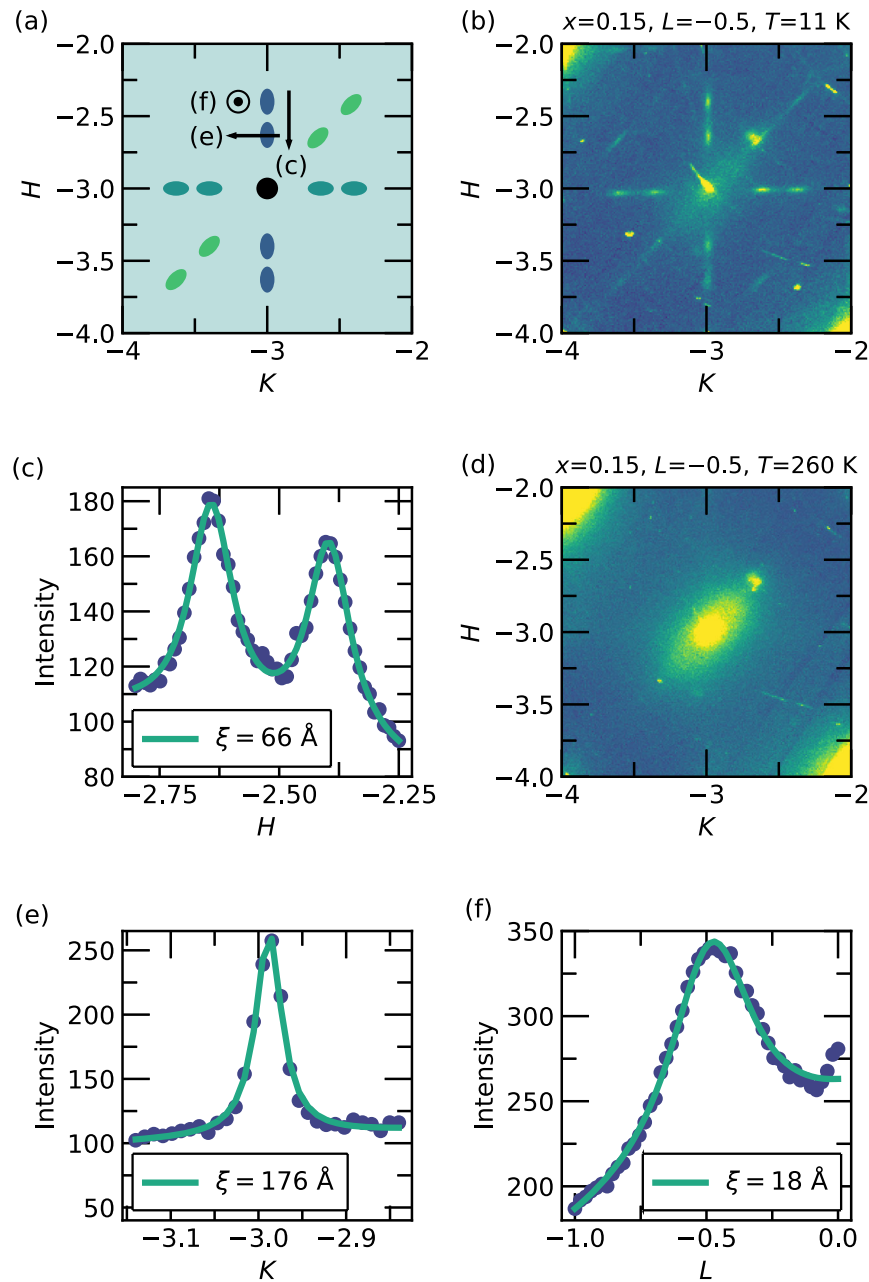


**Fig. 3 X-ray scattering from a  $x = 0.15$  crystal.** **a** Schematic of x-ray scattering in the  $(H, K)$ -plane about a representative zone center for the  $x = 0.15$  sample. Scattering from three domains is illustrated and cut directions for corresponding panels are labeled. **b** Map of x-ray scattering intensities for  $x = 0.15$  at  $T = 11$  K plotted about  $(H, K, -0.5)$  **(c)** One-dimensional cut along  $H$  as illustrated in **(a)**, **(d)** Map of x-ray scattering intensities for  $x = 0.15$  at  $T = 260$  K **(e, f)** One-dimensional cuts along  $K$  and  $L$  as illustrated in **(a)**. Solid lines are the results of pseudo-Voigt fits to the peak lineshapes with the Gaussian component constrained to the instrument's resolution.

downward via hole-doping. In the absence of the reconstructed  $2 \times 2$  cell, the nesting wave vector should be doping dependent, and future studies at higher Sn-concentrations can test this conjecture. Parallels to reported pressure-tuned phase diagrams of  $\text{CsV}_3\text{Sb}_5$  can also be suggested. Both hydrostatic pressure<sup>29,35</sup> and hole-doping<sup>31</sup> have been shown to create 'double dome' type superconducting phase diagrams featuring the rapid suppression of long-range CDW order. A recent NMR study has also suggested the presence of a stripe-like CDW state that emerges in the second superconducting dome once the parent triple-q CDW order is suppressed<sup>36</sup>.

More broadly, our experiments establish  $\text{AV}_3\text{Sb}_5$  as a promising platform for the studies of charge-stripe physics and draw

comparisons with the extensively studied  $4a_0$  charge ordering in cuprates<sup>37</sup>. For example, the sizable doping dependence of charge ordering in Bi-based cuprates<sup>38</sup> appears qualitatively similar to observations in  $\text{CsV}_3\text{Sb}_{5-x}\text{Sn}_x$ . Given the suppression of charge ordering in cuprates in the overdoped regime, it will be of interest to explore the fate of stripe-like correlations in  $\text{CsV}_3\text{Sb}_5$  at an even higher doping level, as samples with higher Sn composition are developed in the future and the multigap superconducting phase is completely suppressed<sup>39</sup>. Initial STM data suggest that, in the low doping regime, the surface wave vector of the quasi-1D correlations evolves with Sn-concentration (Supplementary Figs. 6–8).

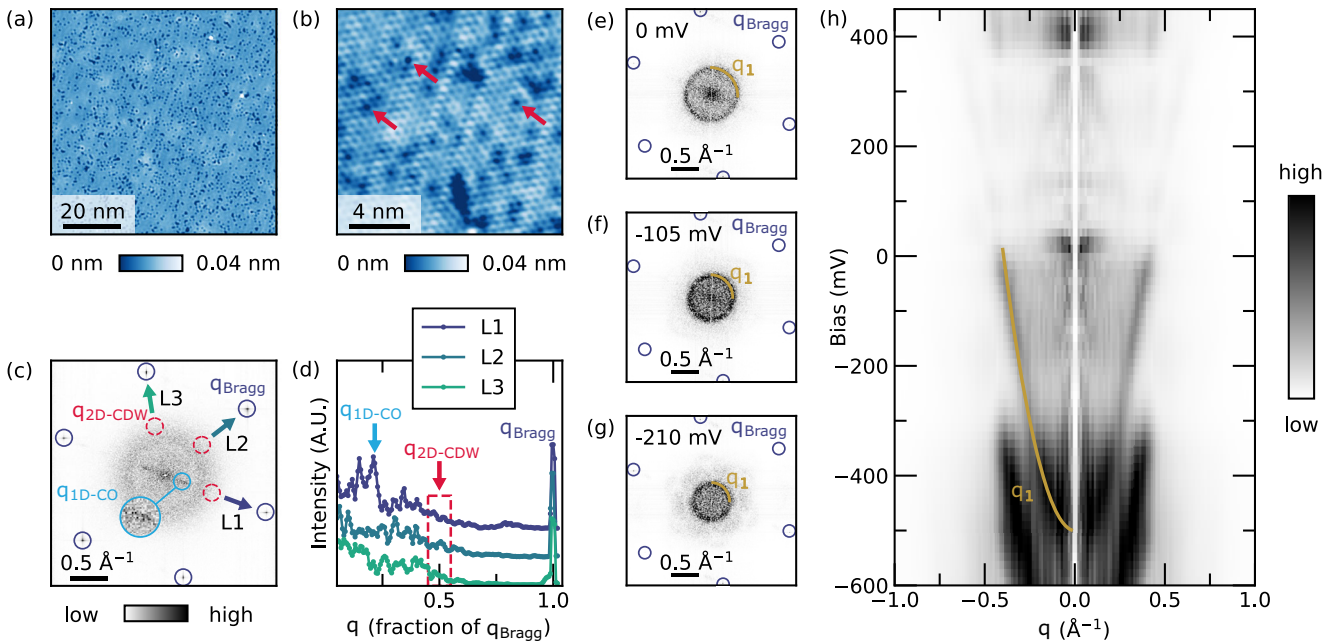


**Fig. 4** Scanning tunneling microscopy data for a  $x = 0.15$  crystal. **a** and **b** show STM topography images of  $\text{CsV}_3\text{Sb}_{5-x}\text{Sn}_x$  with  $x = 0.15$ . Red arrows in **(b)** highlight several representative Sn dopants that can be seen as dark hexagons in the STM topograph, **(c)** Fourier transform of the STM topography showing the presence of quasi-1D,  $\mathbf{q}_{1\text{D-CO}}$  correlations, and the absence of  $2 \times 2$  ( $\mathbf{q}_{2\text{D-CDW}}$ ) correlations, **(d)** One dimensional line cuts through the Fourier map in **(c)**, **(e–g)** Quasiparticle interference spectra collected at 0 mV,  $-105$  mV, and  $-210$  mV biases respectively. The circular scattering from  $\mathbf{q}_1$  due to the Sb  $p_z$  states is marked. **h** The dispersion of the QPI pattern showing the bottom of the Sb  $p_z$  band has risen to  $\approx -500$  meV. Label  $\mathbf{q}_{1\text{D-CO}}$  denotes the momentum-transfer space ( $\mathbf{q}$ -space) position of the 1D CDW wave vector; the label  $\mathbf{q}_{2\text{D-CDW}}$  marks the  $\mathbf{q}$ -space location where FT peaks associated with the  $2 \times 2$  CDW state would be expected.

In summary, our results demonstrate a complex landscape of charge correlations in the hole-doped kagome superconductor  $\text{CsV}_3\text{Sb}_{5-x}\text{Sn}_x$ . Light hole-doping eliminates  $2 \times 2 \times 4$  supercell charge correlations and suppresses long-range interlayer correlations. Continued hole-doping results in the suppression of the  $2 \times 2$  commensurate CDW state and the striking stabilization of quasi-1D, incommensurate charge correlations. These emergent, quasi-1D correlations demonstrate an underlying electronic rotational symmetry breaking present across the phase diagram of this system and are suggestive of a  $2\mathbf{k}_F$  nesting instability at the Fermi surface. These results provide important experimental insights into competing charge correlations in the class of  $\text{AV}_3\text{Sb}_5$  superconductors and crucial input for modeling the unconventional interplay between charge density wave order and the low-temperature superconducting ground state.

## METHODS

### Crystal growth

$\text{CsV}_3\text{Sb}_{5-x}\text{Sn}_x$  crystals with  $x = 0.025$  and  $x = 0.15$  were made with a flux of  $\text{Cs}_{20}\text{V}_{15}\text{Sb}_{90}\text{Sn}_{30}$  and  $\text{Cs}_{20}\text{V}_{15}\text{Sb}_{106}\text{Sn}_{34}$  respectively. Fluxes were ball-milled for 60 mins and then packed into alumina crucibles, and sealed under inert atmosphere within stainless steel tubes. Tubes were heated to  $1000^\circ\text{C}$  and kept at  $1000^\circ\text{C}$  for 12 h and then cooled quickly to  $900^\circ\text{C}$ , and then slowly cooled ( $2^\circ\text{C}/\text{hour}$ ) to  $500^\circ\text{C}$ . Undoped  $x = 0$  crystals were grown using the method previously reported<sup>2</sup>.

### Single crystal X-ray diffraction

Temperature-dependent synchrotron x-ray diffraction were collected at the ID4B (QM2) beamline, CHESS. In ID4B measurements, temperature was controlled by a stream of cold helium gas flowing across the single-crystal sample. An incident x-ray of energy  $26$  keV ( $\lambda = 0.6749 \text{ \AA}$ ) was selected using a double-bounce diamond monochromator. Bragg reflections were collected in

transmission mode, and the sample was rotated with full  $360^\circ$  patterns, sliced into  $0.1^\circ$  frames.

### Scanning tunneling microscopy measurements

STM data were acquired using a Unisoku USM1300 STM at approximately  $4.5$  K. Spectroscopic measurements were made using a standard lock-in technique with  $915$  Hz frequency and bias excitation. STM tips were custom-made chemically-etched tungsten tips, annealed in UHV to bright orange color prior to the measurements.

### Optical pump-probe reflectivity measurements

Optical pump-probe reflectivity measurements similar to those in Ratcliff et al.<sup>26</sup> were performed on a cleaved single crystal of nominal composition  $\text{CsV}_3\text{Sb}_{4.8}\text{Sn}_{0.15}$  mounted in an optical cryostat. Pump and probe pulses were linearly polarized in-plane and configured in a cross-polarized geometry, with the pump center wavelength at  $760$  nm and the probe center wavelength at  $800$  nm. The  $\approx 50$  fs optical pulses were incident at a repetition rate of  $250$  kHz with a fluence of  $100 \mu\text{J cm}^{-2}$ . A lock-in amplifier and optical chopper were used to measure the pump-induced transient change in reflectivity of the probe. To isolate coherent phonon oscillations, an exponential background was subtracted from the transient response before Fourier transforming to the frequency domain. Scans at different temperatures were normalized to the intensity of the fully symmetric phonon at  $4.1$  THz.

### DATA AVAILABILITY

All data supporting the findings of this study are available from the corresponding authors upon request.

Received: 18 January 2023; Accepted: 15 July 2023;

Published online: 25 July 2023

## REFERENCES

- Ortiz, B. R. et al. New kagome prototype materials: discovery of  $KV_3Sb_5$ ,  $RbV_3Sb_5$ , and  $CsV_3Sb_5$ . *Phys. Rev. Mater.* **3**, 094407 (2019).
- Ortiz, B. R. et al.  $CsV_3Sb_5$ : A Z2 topological kagome metal with a superconducting ground state. *Phys. Rev. Lett.* **125**, 247002 (2020).
- Ortiz, B. R. et al. Superconductivity in the Z2 kagome metal  $KV_3Sb_5$ . *Phys. Rev. Mater.* **5**, 034801 (2021).
- Yin, Q. et al. Superconductivity and normal-state properties of kagome metal  $RbV_3Sb_5$  single crystals. *Chin. Phys. Lett.* **38**, 037403 (2021).
- Chen, H. et al. Roton pair density wave in a strong-coupling kagome superconductor. *Nature* **599**, 222–228 (2021).
- Ge, J. et al. Discovery of charge-4e and charge-6e superconductivity in kagome superconductor  $CsV_3Sb_5$ . Preprint at <https://arxiv.org/abs/2201.10352> (2022).
- Guo, C. et al. Switchable chiral transport in charge-ordered kagome metal  $CsV_3Sb_5$ . *Nature* **611**, 461–466 (2022).
- Wu, Y. et al. Nonreciprocal charge transport in topological kagome superconductor  $CsV_3Sb_5$ . *npj Quant. Mater.* **7**, 105 (2022).
- Xu, Y. et al. Three-state nematicity and magneto-optical kerr effect in the charge density waves in kagome superconductors. *Nat. Phys.* **18**, 1470–1475 (2022).
- Mielke, C. et al. Time-reversal symmetry-breaking charge order in a kagome superconductor. *Nature* **602**, 245–250 (2022).
- Yu, L. et al. Evidence of a hidden flux phase in the topological kagome metal  $CsV_3Sb_5$ . Preprint at <https://arxiv.org/abs/2107.10714> (2021).
- Guo, C. et al. Switchable chiral transport in charge-ordered kagome metal  $CsV_3Sb_5$ . *Nature* **611**, 461–466 (2022).
- Jiang, Y.-X. et al. Unconventional chiral charge order in kagome superconductor  $KV_3Sb_5$ . *Nat. Mater.* **20**, 1353–1357 (2021).
- Zhao, H. et al. Cascade of correlated electron states in the kagome superconductor  $CsV_3Sb_5$ . *Nature* **599**, 216–221 (2021).
- Shumiya, N. et al. Intrinsic nature of chiral charge order in the kagome superconductor  $RbV_3Sb_5$ . *Phys. Rev. B* **104**, 035131 (2021).
- Park, T., Ye, M. & Balents, L. Electronic instabilities of kagome metals: saddle points and landau theory. *Phys. Rev. B* **104**, 035142 (2021).
- Tan, H., Liu, Y., Wang, Z. & Yan, B. Charge density waves and electronic properties of superconducting kagome metals. *Chin. Phys. Lett.* **127**, 046401 (2021).
- Liang, Z. et al. Three-dimensional charge density wave and surface-dependent vortex-core states in a kagome superconductor  $CsV_3Sb_5$ . *Phys. Rev. X* **11**, 031026 (2021).
- Ortiz, B. R. et al. Fermi surface mapping and the nature of charge-density-wave order in the kagome superconductor  $CsV_3Sb_5$ . *Phys. Rev. X* **11**, 041030 (2021).
- Li, H. et al. Observation of unconventional charge density wave without acoustic phonon anomaly in kagome superconductors  $AV_3Sb_5$  (A = Rb, Cs). *Phys. Rev. X* **11**, 031050 (2021).
- Christensen, M. H., Birol, T., Andersen, B. M. & Fernandes, R. M. Theory of the charge density wave in  $AV_3Sb_5$  kagome metals. *Phys. Rev. B* **104**, 214513 (2021).
- Kang, M. et al. Charge order landscape and competition with superconductivity in kagome metals. *Nat. Mater.* **22**, 186–193 (2023).
- Hu, Y. et al. Coexistence of trihexagonal and star-of-david pattern in the charge density wave of the kagome superconductor  $AV_3Sb_5$ . *Phys. Rev. B* **106**, L241106 (2022).
- Stahl, Q. et al. Temperature-driven reorganization of electronic order in  $CsV_3Sb_5$ . *Phys. Rev. B* **105**, 195136 (2022).
- Xiao, Q. et al. Coexistence of multiple stacking charge density waves in kagome superconductor  $CsV_3Sb_5$ . *Phys. Rev. Res.* **5**, L012032 (2023).
- Ratcliff, N. et al. Coherent phonon spectroscopy and interlayer modulation of charge density wave order in the kagome metal  $CsV_3Sb_5$ . *Phys. Rev. Mater.* **5**, L111801 (2021).
- Wu, S. et al. Charge density wave order in the kagome metal  $AV_3Sb_5$  (A = Cs, Rb, K). *Phys. Rev. B* **105**, 155106 (2022).
- Luo, J. et al. Possible star-of-david pattern charge density wave with additional modulation in the kagome superconductor  $CsV_3Sb_5$ . *npj Quant. Mater.* **7**, 1–7 (2022).
- Chen, K. et al. Double superconducting dome and triple enhancement of  $T_c$  in the kagome superconductor  $CsV_3Sb_5$  under high pressure. *Phys. Rev. Lett.* **126**, 247001 (2021).
- Yu, F. et al. Unusual competition of superconductivity and charge-density-wave state in a compressed topological kagome metal. *Nat. Commun.* **12**, 1–6 (2021).
- Oey, Y. M. et al. Fermi level tuning and double-dome superconductivity in the kagome metal  $CsV_3Sb_{5-x}Sn_x$ . *Phys. Rev. Mater.* **6**, L041801 (2022).
- Li, H. et al. Rotation symmetry breaking in the normal state of a kagome superconductor  $KV_3Sb_5$ . *Nat. Phys.* **18**, 265–270 (2022).
- LaBollita, H. & Botana, A. S. Tuning the van hove singularities in  $AV_3Sb_5$  (A = K, Rb, Cs) via pressure and doping. *Phys. Rev. B* **104**, 205129 (2021).
- Li, H. et al. Unidirectional coherent quasiparticles in the high-temperature rotational symmetry broken phase of  $AV_3Sb_5$  kagome superconductors. *Nat. Phys.* **19**, 637–643 (2023).
- Yu, F. H. et al. Unusual competition of superconductivity and charge-density-wave state in a compressed topological kagome metal. *Nat. Commun.* **12**, 3645 (2021).
- Zheng, L. et al. Emergent charge order in pressurized kagome superconductor  $CsV_3Sb_5$ . *Nature* **611**, 682–687 (2022).
- Comin, R. & Damascelli, A. Resonant x-ray scattering studies of charge order in cuprates. *Annu. Rev. Condens. Matter Phys.* **7**, 369–405 (2016).
- da Silva Neto, E. H. et al. Ubiquitous interplay between charge ordering and high-temperature superconductivity in cuprates. *Science* **343**, 393–396 (2014).
- Gupta, R. et al. Microscopic evidence for anisotropic multigap superconductivity in the  $CsV_3Sb_5$  kagome superconductor. *npj Quant. Mater.* **7**, 49 (2022).

## ACKNOWLEDGEMENTS

This work was supported by the National Science Foundation (NSF) through Enabling Quantum Leap: Convergent Accelerated Discovery Foundries for Quantum Materials Science, Engineering and Information (Q-AMASE-i): Quantum Foundry at UC Santa Barbara (DMR-1906325). I.Z. gratefully acknowledges the support from the National Science Foundation grant NSF-DMR 2216080. Z.W. is supported by U.S. Department of Energy, Basic Energy Sciences Grant No. DE-FG02-99ER45747 and the Cottrell SEED Award No. 27856 from Research Corporation for Science Advancement. The research reported here made use of shared facilities of the NSF Materials Research Science and Engineering Center at UC Santa Barbara DMR-1720256, a member of the Materials Research Facilities Network ([www.mrfn.org](http://www.mrfn.org)). This work is based upon research conducted at the Center for High Energy X-ray Sciences (CHEXS) which is supported by the National Science Foundation under award DMR-1829070. Any opinions, findings, and conclusions or recommendations expressed in this material are those of the authors and do not necessarily reflect the views of the National Science Foundation.

## AUTHOR CONTRIBUTIONS

Y.M.O. and B.R.O. synthesized the studied materials. Y.M.O., B.R.O., G.P., and J.R. collected the X-ray diffraction data. L.K. analyzed the X-ray diffraction data. The STM experiments were conducted by H.L., Z.R., and Z.W. I.Z. contributed to the interpretation of the STM data. Optical pump-probe reflectivity measurements were performed by T.K. and J.W.H. S.D.W. designed the study and R.S. contributed to the paper review. S.D.W. and L.K. wrote the paper.

## COMPETING INTERESTS

The authors declare no competing interests.

## ADDITIONAL INFORMATION

**Supplementary information** The online version contains supplementary material available at <https://doi.org/10.1038/s41535-023-00570-x>.

**Correspondence** and requests for materials should be addressed to Stephen D. Wilson.

**Reprints and permission information** is available at <http://www.nature.com/reprints>

**Publisher's note** Springer Nature remains neutral with regard to jurisdictional claims in published maps and institutional affiliations.



**Open Access** This article is licensed under a Creative Commons

Attribution 4.0 International License, which permits use, sharing, adaptation, distribution and reproduction in any medium or format, as long as you give appropriate credit to the original author(s) and the source, provide a link to the Creative Commons license, and indicate if changes were made. The images or other third party material in this article are included in the article's Creative Commons license, unless indicated otherwise in a credit line to the material. If material is not included in the article's Creative Commons license and your intended use is not permitted by statutory regulation or exceeds the permitted use, you will need to obtain permission directly from the copyright holder. To view a copy of this license, visit <http://creativecommons.org/licenses/by/4.0/>.